Measurement of pion photoproduction at threshold on ^{6}Li†

G. Audit, A. Bloch, N. de Botton, C. Schuhl, G. Tamas, and C. Tzara
DPhN/HE, Centre d'Etudes Nucléaires de Saclay, 91190 Gif-sur-Yvette, France

J. Deutsch, D. Favart, R. Prieels, and B. Van Oystaeyen
Institut de Physique Corpusculaire, Université Catholique de Louvain, B-1348 Louvain-la-Neuve, Belgium

(Received 13 December 1976)

We remeasured with improved techniques the positive-pion photoproduction yield on ^{6}Li near threshold and up to 7.2 MeV above it. If the total cross section of the reaction $\gamma+p\rightarrow\pi^++n$ is expressed as $\sigma_p=aq/k$, our result for the reaction $\gamma+{}^6\mathrm{Li}\rightarrow\pi^++{}^6\mathrm{He}_{g.s.}$ near threshold is

$$\sigma_{\mathrm{Li}}=(0.098\pm0.004)(aq/k)\{(12.5/q)/[\exp(12.5/q)-1]\},$$

where q is the pion and k the photon c.m. momenta expressed in units of MeV/c. Deviations from this expression above threshold and the contribution of $\gamma+{}^6\mathrm{Li}\rightarrow\pi^++{}^6\mathrm{He}$ (1.8 MeV) were also observed. The full understanding of this result requires further theoretical work and complementary experiments on the $A=6$ nuclear system.

[NUCLEAR REACTIONS $^6\mathrm{Li}(\gamma,\pi^+)^6\mathrm{He}_{g.s.}$ and ^{6}He (1.8 MeV), E_{π^+}: 0–7 MeV, measured σ relative to proton target.]

I. INTRODUCTION

The pion photoproduction on a nucleus $\gamma+i\rightarrow\pi+f$ can be viewed as a transition induced by a photon of momentum k from a nuclear ground state i to a peculiar excited state consisting of a pion and the nuclear state f. In the vicinity of threshold ($k\simeq m_\pi$), the photoproduced pion interacts quite weakly with the nucleus as witnessed by the relatively small width of pionic 1s states in light nuclei. As the pion wavelength ($1/q$) is much larger than the nuclear radius R, the pion wave function $\psi_\pi(\vec{r})$ can be considered as a constant over the nuclear volume and the transition amplitude will have the form: $\psi_\pi(0)\langle f|e^{i\vec{k}\vec{r}}O|i\rangle$.

For a nucleon, near threshold the operator O reduces to the simple spin-flip term $E_{0+}(\vec{\sigma}\cdot\vec{\epsilon})$. ($\vec{\epsilon}$ is the photon polarization unit vector.) Deviations from this limit can be predicted by low-energy theorems and the partially conserved axial-vector current (PCAC) hypothesis.[1] The application of this approach to a *nuclear* system is much less clear-cut,[2–4] so instead a microscopic description is generally adopted. Other ingredients than the structure of $|i\rangle$ and $|f\rangle$ enter the microscopic approach: the elementary interaction amplitude rewritten in the photon-nucleus center-of-mass system, eventually modified to account for many-body effects[2,4]; the distortion of the pion field by the Coulomb and strong interactions with the nucleus. To the extent that these effects are under control, radiative pion capture from s orbits or pion photoproduction at threshold will explore the axial part of the nuclear transition $i\rightarrow f$ in complement to the electromagnetic and weak interaction probes.

Even though radiative capture has been extensively studied,[5,6] it is plagued by the multiplicity of Bohr orbits from which the capture may occur; it is only recently that the development of new techniques allows hope for identification of 1s capture.[7] In view of this situation, we developed a method to measure, with an accuracy of a few percent, the photoproduction of positive pions. The photoproduction is performed near enough to the threshold to render all but $l=0$ partial waves practically negligible.[8] In this energy region the cross section of the process between discrete nuclear states i and f is conveniently parametrized by

$$\sigma=a(i\rightarrow f)Sq/k\,. \tag{1}$$

Here q and k are the pion and photon momenta in the center-of-mass system. We factorized out the main contribution to the variation of $\sigma k/q$ near threshold:

$$S=2\pi\gamma/(e^{2\pi\gamma}-1)\quad(\text{where }\gamma=Ze^2/\hbar v)$$

describing the effect of the Coulomb repulsion between the pion of velocity v and the nucleus of charge Z assumed to be pointlike.[9] The remaining quantity $a(i\rightarrow f)$ contains, in addition to the nuclear-physics information, the distortion of the pion wave by the strong interaction of the nucleus and the finite extension of the nuclear charge.

We measure the nuclear photoproduction cross section relative to the one on the proton. So our

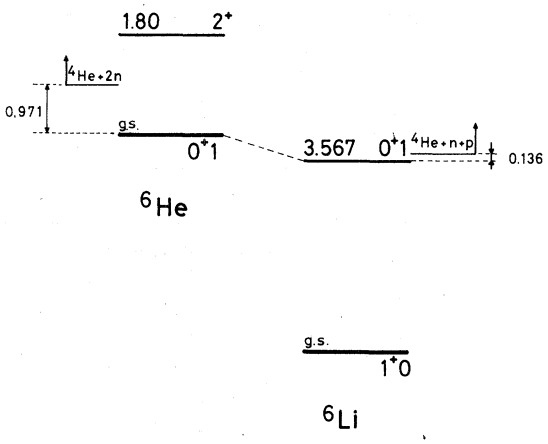

FIG. 1. Characteristics of the $A = 6$ system relevant to the experiment (excitation energies in MeV).

result can be expressed as the ratio

$$a(i \to f)/a(p \to n) .$$

The method was first applied to the $\gamma + {}^6\mathrm{Li} \to \pi^+ + {}^6\mathrm{He}$(g.s.) transition and yielded a result[10] in strong disagreement with an early theoretical prediction.[8] This disagreement prompted a wealth of theoretical efforts to criticize the assumptions entering these predictions and to resolve the discrepancy. The uncertainties in the distortion of the outcoming pion wave due to strong interaction, i.e., the π^+-^{6}He optical potential, tailored to satisfy the ^{6}Li and ^{7}Li pionic x-ray data, were investigated by Cannata, Lucas, and Werntz,[11] who showed that even large unrealistic changes in the optical potential would produce only small effects on the cross section.

Bergström, Auer, and Hicks[12] have reexamined the $M1$ electroexcitation of ^{6}Li(3.56 MeV) analogous to the ^{6}He ground state; they found phenomenological nuclear transition densities which fit the data better than the harmonic oscillator radial wave functions employed previously. The use of these densities and alterations in the configuration mixing of the $T = 1$ levels lead to a sizable decrease of the ratio $a(\mathrm{Li} \to {}^6\mathrm{He})/a(p \to n)$. It was noted also that the spatial extension of the ^{6}He(g.s.) may be smaller than that of its analog ^{6}Li(3.56 MeV),[13] because ^{6}He(g.s.) is more bound than ^{6}Li(3.56 MeV) (Fig. 1). This would presumably lead to a higher cross section than the predicted one.[11] Delorme and Figureau, taking in account momentum dependent terms, found an increase of the cross section by about 10%.

In the mean time it was established that some systematic errors had been overlooked in the first experiment, and we consequently decided to repeat it.

We describe here the improved experiment (also somewhat enlarged in its domain of energy), discuss the origin of the error in our first measurement, and present our new result.

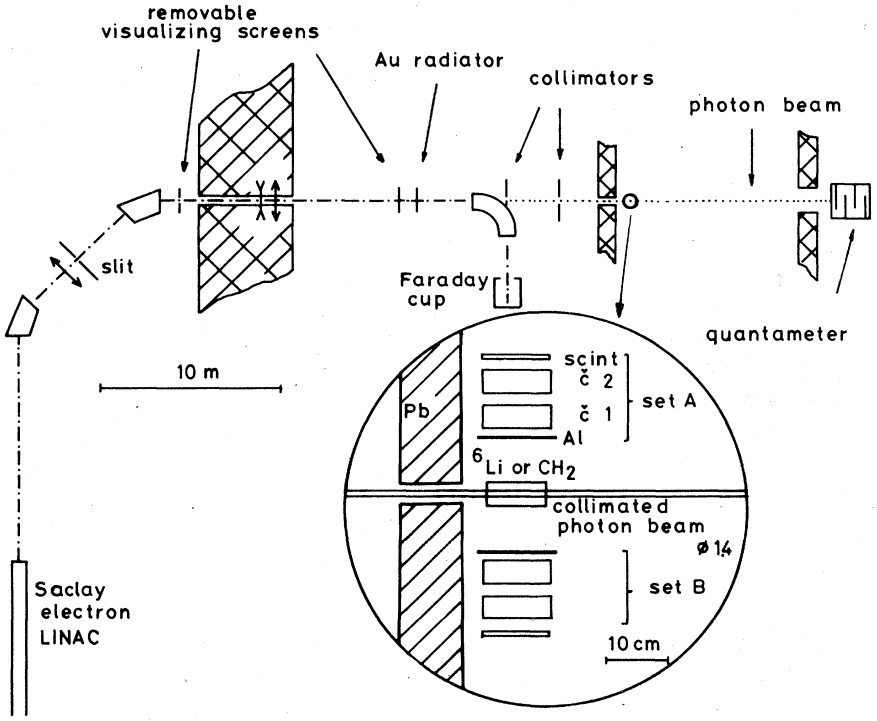

FIG. 2. Layout of the experiment. The insert shows details of the detector system.

II. DESCRIPTION OF THE EXPERIMENT

The experiment consists in the comparison of the π^+ photoproduction yield on ^{6}Li and ^{1}H at comparable excess energies above threshold. The photons are obtained by bremsstrahlung from an electron beam of variable energy; the pions photoproduced and stopped in the target are counted by observing the positrons from their decay muons between the beam bursts. The layout of the experiment is shown in Fig. 2.

A. Beam

The bremsstrahlung beam is derived from a gold converter, 0.01 radiation length thick, hit by electrons from the Accélérateur Linéaire de Saclay. The energy of the electrons is defined by an achromatic beam transport system. The field of the analyzing magnet is measured by proton resonance probe to an accuracy of 10^{-5} yielding a nominal value for this energy. The real energy of the electron is not necessarily the nominal one. The difference, which turned out to be small (cfr. Sec. III C), is practically constant in the range we explore in our experiment (from 145 to 158 MeV). The momentum resolution of the beam $\Delta P/P$, defined by the slits, is between 1.5×10^{-3} and 3.0×10^{-3}. The straggling introduced by the finite converter thickness is small compared to this momentum spread.

The pulses are typically 2 μs wide. Their repetition rate is 2 kHz. Behind the radiator the electrons are swept away by a magnet and their intensity is measured in a Faraday cup. The main collimator restricts the photon beam to a cone of 0.7 mrad around the electron beam axis. The resulting photon beam spot is 1.4 cm in diameter at the target location. An additional collimator protects our detectors against the main collimator halo and the stray particles produced during the beam burst. The photon beam is intercepted by a Wilson-type quantameter. This instrument measures the photon energy flux; the comparison of this flux with the intensity of the electron beam, as measured in the Faraday cup, allows us to monitor any eventual deviation of the incident electron beam from its nominal direction as adjusted originally by visualizing screens. A description of the quantameter and the discussion of its use can be found in Ref. 14.

B. Targets

The main target is a lithium cylinder 4 cm in diameter and 10 cm long, enriched to 94.8% in ^{6}Li and hermetically sealed in a cylindrical stainless steel container of 0.5 mm wall and 0.02 mm window thickness. The ^{6}Li target can be interchanged with a chemically pure granular polyethylene (CH_2) one. The contribution of the target holder to the measured photoproduction yield is totally negligible. The ^{1}H and ^{12}C π^+ photoproduction thresholds are 151.44 and 154.50 MeV, respectively, so that up to 3 MeV above the proton threshold the carbon content of polyethylene does not contribute to the photoproduction yield. Even at higher energies, that contribution remains negligible due to the Coulomb attenuation factor and because, as will be discussed later, the yields increase approximately as the square of the energy above threshold ω. For instance, at 6 MeV above threshold for hydrogen, the contribution of photoproduction from carbon amounts to less than 1% of the total pion yield as deduced from preliminary experiments performed on a ^{12}C target. The density of the polyethylene target ($\rho = 0.400$ g/cm^3) is chosen, by computation, so as to approximately equalize the escape probability of positrons from this target and from the ^{6}Li ($\rho = 0.458$ g/cm^3) one. In order to check this computation, measurements are also made with a CH_2 target of higher density ($\rho = 0.588$ g/cm^3).

C. Detectors

We use two identical detector sets installed symmetrically at 90° to the photon beam (Fig. 2 insert). Each set consists of two 40 mm thick Čerenkov Lucite counters and one 5 mm thick plastic scintillator observed in coincidence. The detection solid angle is defined by the scintillator in order to avoid edge effects in the Čerenkov counter. The first detector is protected by a 5 mm Al sheet from the low-energy background produced in the target during the beam period; in addition to the regular high voltage supply, a booster is used on the three last dynodes of the phototubes mounted on the front detectors.

D. Measuring procedure

The measurements are performed, interchanging the targets, at various electron energies, repeating frequently the same conditions. A measurement consists in counting the number of muon-decay positrons originating from the pions, photoproduced at a fixed beam energy, for a given target and in the determination of the corresponding bremsstrahlung-beam intensity. Positrons are observed during a 26 μs gate, beginning $\simeq$2 μs after the end of the beam burst; the time interval between the start of the gate and the event is measured by means of a time to amplitude converter. A second observation gate of 92 μs, starting $\simeq$75 μs after the beam burst, is used to record the

background associated with other events than μ-decay positrons.

The integral of the bremsstrahlung flux is by no means a sufficient normalization for our purposes. We have to normalize the number of positrons observed to the total number of bremsstrahlung quanta above threshold which hit the target, taking into account the probability for a muon to survive until the beginning of the observation interval. This surviving fraction depends, of course, on the time structure of the beam bursts. In order to perform the normalization, we integrate the quantameter output, according to the "leaky capacitor" method,[15] with a time constant equal to the muon lifetime. The resulting pulses are sampled at the beginning of the observation interval. A second sampling is performed 3 μs after the first one. These samplings are digitized and accumulated in scalers. The difference of the two samplings is used for the normalization in order to cancel the influence of a slight undershoot of the quantameter signal introduced by the differentiation due to capacitive coupling. As an overall check on the correctness of our normalization procedure we are able to show that our normalized positron counting rate stays constant within statistics ($\pm 10^{-2}$), when we shift the observation interval 2 μs further away from the beam burst.

The sequence of the different gates and samplings is shown in Fig. 3.

E. Electronics and data acquisition system

A schematic diagram of the electronics is given in Fig. 4. The circuitry consists of fast electronic modular circuits; its function is to provide to a PDP 8 computer both the trigger for recording an event and the information which characterizes it.

An event is defined by a threefold coincidence from one detector set. The following digitized information is supplied to the computer for each event and subsequently recorded on a magnetic tape: set of detectors hit (A or B); time interval between the opening of the observation gate and the occurrence of the event; pulse heights in the three detectors. On line the following spectra are constructed for each set of detectors: time distribution histogram of the events (Fig. 5) which displays the characteristic lifetime of the muon; pulse-height spectra of the events in the three detectors which are used to check the overall stability. In Fig. 6 we show characteristic spectra of the Čerenkov detectors, demonstrating their stability against the interchange of the ^{6}Li and CH_2 targets.

III. ANALYSIS OF THE DATA

A. Data reduction

The bidimensional plots of the pulse amplitudes for a given run in the two Čerenkov counters for both sets are constructed for each run. They reveal the presence of a background characterized by small pulse heights in both Čerenkov counters.

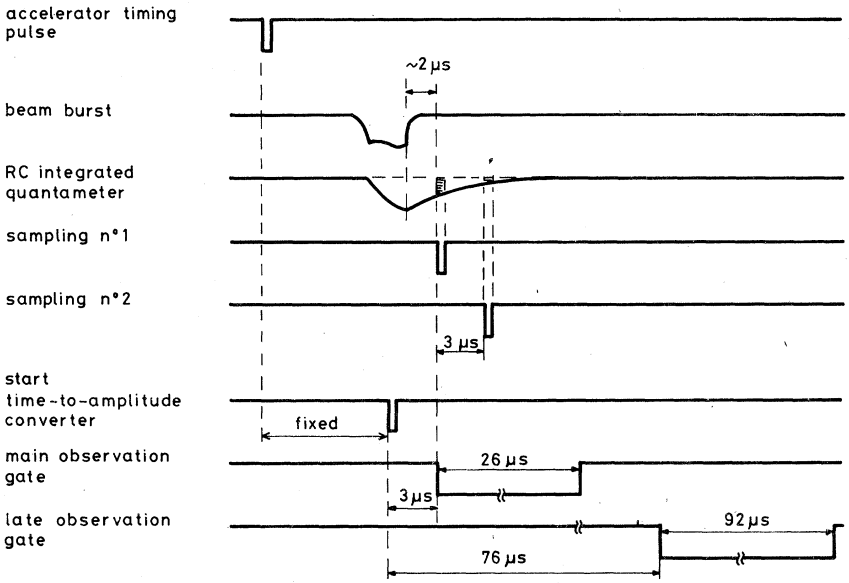

FIG. 3. Timing sequence of the experiment.

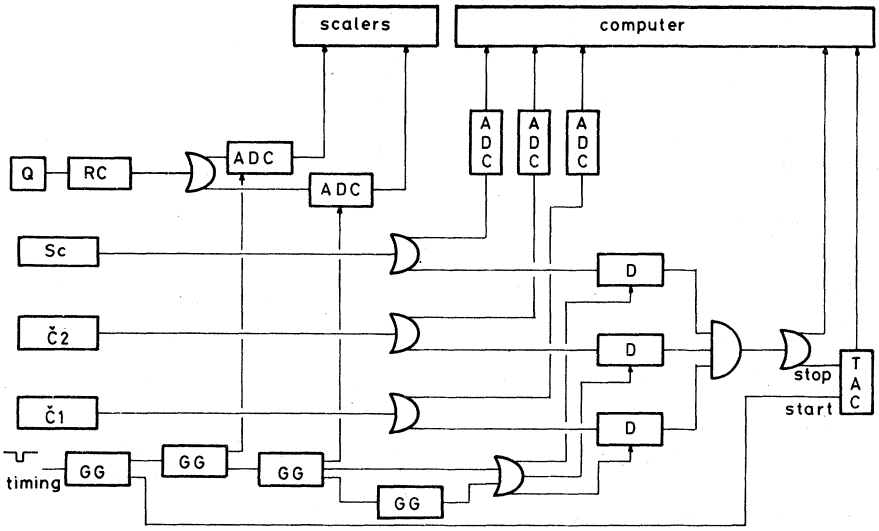

FIG. 4. Schematic diagram of the electronics (only one detector-set is shown). RC: "leaky capacitor" integrator; Sc: scintillator; Č1 and Č2: Čerenkov detectors; GG: gate generator; ADC: analog to digital converter; D: gated discriminator; TAC: time-to-amplitude converter; Q: quantameter.

The position of the valley separating the background from good events is clearly seen and stability of its position is checked throughout the experiment.

We show in Fig. 7 such distributions obtained below and above photoproduction threshold in the main gate. For the scintillator, the pulse-height distributions of the good events and those of the background are not significantly different; consequently this distribution could not be used for further background rejection. Only the first 6 μs of the main observation gate are retained and the events are selected according to the criterium that the sum of the pulse amplitudes in the two Čerenkov detectors should be larger than a given threshold T; the complete analysis is performed using different values of T.

Measurements performed below photoproduction threshold show the presence of a few high amplitude residual events which could not be removed by any reasonable choice of T and display an essentially constant time distribution. We assume that this time distribution is independent of the beam energy in the small energy range we investigated. Consequently, we use the subthreshold measurements to determine, for each target, the ratio of

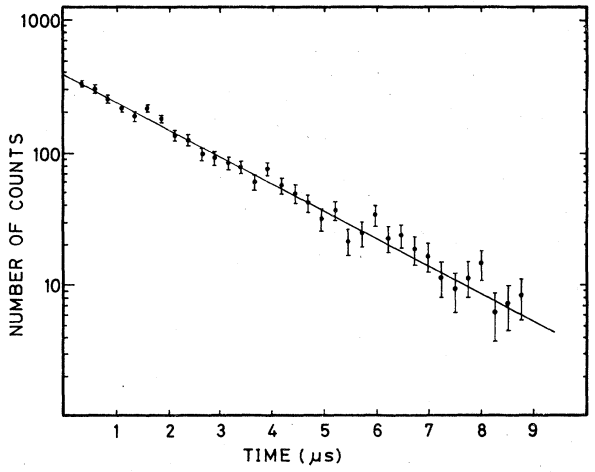

FIG. 5. Typical time distribution of the events. The line is a fit to the data yielding the correct muon lifetime.

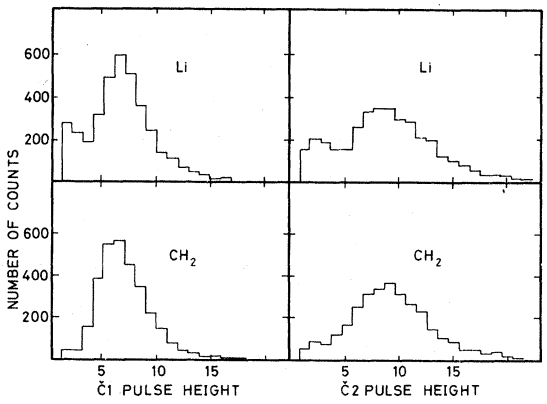

FIG. 6. Characteristic amplitude spectra of the Čerenkov detectors exposed to Li and to CH_2 targets.

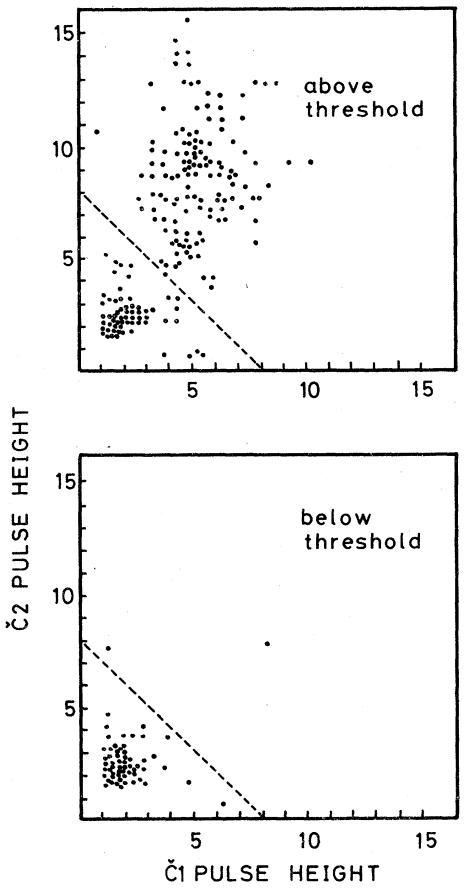

FIG. 7. Bidimensional amplitude distribution of typical events in the Čerenkov detectors of a set. A cut value $\check{C}_1+\check{C}_2 \equiv T = cte$ is also shown.

this background as measured in the main and late gates. One may notice that within statistics, this ratio is the same for both targets. Multiplying then the number of counts in the late gate by this ratio, we obtain the residual background to be subtracted for each measurement performed above threshold. For a reasonable value of the cut T, the background amounts to 20% of the events in the conditions of the lowest counting rate (^{6}Li, 1 MeV above threshold). Thanks to our threefold coincidence requirement, the accidentals rate is entirely negligible.

After subtraction of the background, we obtain the yields normalized as explained in Sec. II D to the difference between the two digitized samplings of the quantameter output signal divided by the incident electron energy E_e. (The quantameter measures the total energy flux, which is proportional, in good approximation, to the incident electron energy E_e.) The photoproduction yields per target nucleus, obtained with a suitable value for the cut as explained in Sec. III C are presented in Table I. The stated errors are obtained by

TABLE I. Photoproduction yield per nucleus, in arbitrary units, for different values of the nominal bremsstrahlung end-point energy both for the ^{6}Li and CH_2 targets.

E_e	Set A	Set B
	$A_p(E_e)$	
152.5	0.099 ± 0.011	0.095 ± 0.010
153	0.334 ± 0.011	0.331 ± 0.010
154	1.087 ± 0.023	1.123 ± 0.023
155	2.366 ± 0.066	2.264 ± 0.064
157	5.729 ± 0.141	5.417 ± 0.135
158	7.950 ± 0.198	8.415 ± 0.206
	$A_{Li}(E_e)$	
147	0.020 ± 0.002	0.024 ± 0.002
147.5	0.040 ± 0.004	0.032 ± 0.003
148	0.082 ± 0.005	0.079 ± 0.005
149	0.168 ± 0.011	0.178 ± 0.012
150	0.322 ± 0.019	0.363 ± 0.021
153	1.194 ± 0.040	1.153 ± 0.036

combining the statistical ones with the uncertainties induced by a possible fluctuation of the average electron momentum. This fluctuation is estimated to ±10% of the beam momentum spread, e.g., ≃45 keV at $\Delta P/P = 0.3\%$.

The influence of these possible fluctuations on the yield is estimated assuming a quadratic dependence of the latter on ω, the excess energy above threshold. Using these errors, the reproducibility of the different results obtained for identical beam setting and targets is satisfactory.

B. Relation between the yield and the photoproduction cross section

For a value E_e of the end-point energy of the photon spectrum, the observed yield per nucleus is

$$A(E_e) = \frac{\epsilon\Omega}{4\pi} \int_{E_0}^{E_e} \sigma(E) B(E, E_e) dE$$

$$= \frac{\epsilon\Omega}{4\pi} a(i \to f) I(E_e),$$

where E_0 is the threshold laboratory photon energy; $\sigma(E)$ is the π^+ photoproduction cross section at laboratory photon energy E as approximated near threshold by relation (1); $B(E, E_e)$ is the photon spectrum for an average incident electron energy E_e; $\epsilon\Omega/4\pi$ is the total detection efficiency (detection efficiency × solid angle). It should be stressed that due to our precautions $\epsilon\Omega$ is nearly independent of the target (cfr. Sec. III C) and is practically constant in the energy interval we covered. Expressing $\epsilon\Omega$ as $\epsilon\Omega \propto [1 - C(E - E_0)^2]$, Monte Carlo simulation of the process yields

$C_{Li} = 3.3 \times 10^{-4}$ MeV^{-2} and $C_{CH_2} = 1.0 \times 10^{-3}$ MeV^{-2}. The influence of this variation is negligible for the low-energy data; even though this correction remains within the statistical accuracy for the high-energy ones (Sec. III D), it was taken into account.

We perform a numerical evaluation of the quantity

$$I(E_e) = \int_{E_0}^{E_e} \frac{q}{k} SB(E, E_e) dE$$

for both target nuclei as a function of E_e. Due to the smearing of the bremsstrahlung angular distribution induced by the multiple scattering of the incident electrons in the converter, we use the radiation cross section integrated over all emission angles. For this cross section we assume the form derived by Jabbur and Pratt in Ref. 16. This form approaches the one derived by Bethe and Heitler, except near end point where it takes the correct value computed by the same authors in another paper.[17] In the evaluation of the integral $I(E_e)$, we allow for the energy loss in the converter and for the finite energy distribution of the incident electrons, assumed to be of rectangular shape of a width depending on the opening of the analyzing slits.

C. Extraction of the ratio $a(^6\text{Li} \to {}^6\text{He})/a(p \to n)$

An absolute measurement of $a(i \to f)$ would require the knowledge of $\epsilon\Omega$ and an experimental test of $B(E, E_e)$ near end point. However, by performing a relative measurement of $a(i \to f)/a(p \to n)$ we circumvent the first requirement and also minimize to a large extent the influence of the uncertainties in the end-point region of the bremsstrahlung spectrum as it will be shown below. In order to extract $a(^6\text{Li} \to {}^6\text{He})/a(p \to n)$ we restrict ourselves to the excess energy region above threshold ($0 < \omega < 2$ MeV) where the approximate expression (1) of the cross section is valid.

The cross section deviates from the approximate expression [i.e., $a(^6\text{Li} \to {}^6\text{He})/a(p \to n)$ is not constant] because of the variation with energy of: (1) the nuclear matrix element; (2) the elementary amplitudes; (3) the pion wave central density compared to the average one. These corrections are model dependent. Their overall effect can be parametrized as $a(^6\text{Li} \to {}^6\text{He})/a(p \to n) \simeq [a(^6\text{Li} \to {}^6\text{He})/a(p \to n)_{\text{thresh}}][1 - (b_{Li} - b_p)\omega]$. In order to illustrate the smallness of this correction, let us assume with Delorme and Figureau[18]: $b_{Li} - b_p = 10^{-2}$ MeV^{-1}, compatible with our results obtained at higher energies above threshold (cfr. Sec. III D). The correction $b\omega$ turns out to be of the order of 10^{-2} and thus small compared to the precision of our result.

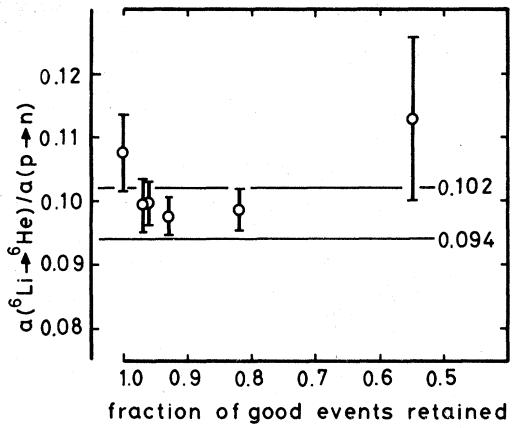

FIG. 8. Dependence of the result a_{Li}/a_p on the cut applied to the detector pulse height $C_1 + C_2 \equiv T$ expressed as the fraction of good events retained. The error limits of our final result are also represented.

The experimental yields normalized to the number of target nuclei and to the effective photon intensity, such as those presented for a given value of the cut T in Table I, can be expressed for each set of detectors as

$$A_p(E_e) = K I_p(E_e + \Delta E_e)$$

$$A_{Li}(E_e) = K[a(^6\text{Li} \to {}^6\text{He})/a(p \to n)] I_{Li}(E_e + \Delta E_e),$$

where $K = (\epsilon\Omega/4\pi) a(p \to n)$ and ΔE_e is the difference between the nominal electron energies listed in Table I and the unknown real ones. $a(^6\text{Li} \to {}^6\text{He})/a(p \to n)$ is extracted, considering independently the two sets of detectors, for different values of the cut T.

In order to illustrate the constancy of our results against the variation of the cuts we display in Fig. 8 $a(^6\text{Li} \to {}^6\text{He})/a(p \to n)$ as a function of the fraction of events retained for both detectors in the cutting procedure. It is worthwhile to note that the normalized χ^2 for these fits stayed between 0.85 and 1.10.

The value $a(^6\text{Li} \to {}^6\text{He})/a(p \to n)$ is very unsensitive to the bremsstrahlung shape near the end point: changing the assumed form of $B(E, E_e)$ for the Bethe-Heitler one, the value of ΔE_e changes from -425 keV to -300 keV but $a(^6\text{Li} \to {}^6\text{He})/a(p \to n)$ stays constant within 10^{-3}.

A small correction has to be applied to $a(^6\text{Li} \to {}^6\text{He})/a(p \to n)$ due to the differences in the escape probabilities of the positrons from the used targets. This correction is deduced from an auxiliary measurement performed with the dense CH_2 target and found to be $(0.3 \pm 0.3)\%$. We also consider the effects of the photon absorption in the target which is slightly different, in each target, for the total spectrum as measured by the quantameter and for its high-energy fraction relevant for

the π^+ photoproduction process. This correction on $a(^6\text{Li} \rightarrow {}^6\text{He})/a(p \rightarrow n)$ amounts to 0.5%. Our final result is

$$a(^6\text{Li} \rightarrow {}^6\text{He})/a(p \rightarrow n) = 0.098 \pm 0.004.$$

D. Analysis of the higher excitation energy data

Using the values of $a_p(\epsilon\Omega/4\pi)$, ΔE_e, and $a(^6\text{Li} \rightarrow {}^6\text{He})/a(p \rightarrow n)$ as extracted from the near threshold subset of our data, we analyze the whole body of our measurements by using the following expression for the cross section:

$$\sigma = a(^6\text{Li} \rightarrow {}^6\text{He})(1 - b_{\text{Li}}\omega)S\frac{q}{k} + a(^6\text{Li} \rightarrow {}^6\text{He}^*)S'\frac{q'}{k}. \tag{2}$$

ω is the excess energy of the beam above ^{6}He(g.s.) threshold. The primed quantities refer to the ^{6}He(1.8 MeV) resonance, which is assumed to exhaust all the excitation of the continuum in the region, as shown in the radiative pion capture experiment.[6] We assumed $b'_{\text{Li}} = 0$.

A least squares fit yields:

$$b_p = (6.3 \pm 2.9) \times 10^{-3}\ \text{MeV}^{-1}$$

to be compared with $b_p = 11 \times 10^{-3}\ \text{MeV}^{-1}$ as given by the Chew-Goldberger-Low-Nambu (CGLN) theory.[18] Note that if we adopt a Bethe-Heitler photon spectrum, this value becomes $(10.6 \pm 2.9) \times 10^{-3}\ \text{MeV}^{-1}$. The same fit gives also:

$$a(^6\text{Li} \rightarrow {}^6\text{He}^*)/a(^6\text{Li} \rightarrow {}^6\text{He}) = 0.70 \pm 0.24$$

and

$$b_{\text{Li}} = (23 \pm 26) \times 10^{-3}\ \text{MeV}^{-1}.$$

These two quantities are strongly correlated ($r = 0.98$) as they are essentially determined by the measurement at the highest value of ω. They compare fairly well with the values obtained by Delorme and Figureau:

$$a(^6\text{Li} \rightarrow {}^6\text{He}^*)/a(^6\text{Li} \rightarrow {}^6\text{He}) = 0.68,$$

and

$$b_{\text{Li}} = 21 \times 10^{-3}\ \text{MeV}^{-1}.$$

Cammarata and Donnelly predict a much larger value of b_{Li}: $b_{\text{Li}} = 40 \times 10^{-3}\ \text{MeV}^{-1}$ and use $b_p = 5 \times 10^{-3}\ \text{MeV}^{-1}$. Such a value of b_{Li} leads to:

$$a(^6\text{Li} \rightarrow {}^6\text{He}^*)/a(^6\text{Li} \rightarrow {}^6\text{He}) = 0.80 \pm 0.30.$$

In Fig. 9 we show the global fit with all our experimental data. Using Eq. (2), our experimental values of the parameters $a(^6\text{Li} \rightarrow {}^6\text{He})$, $a(\text{Li} \rightarrow {}^6\text{He}^*)$, and b_{Li}, and the measured slope of the photoproduction cross section on hydrogen[19]

$$a(p \rightarrow n) = (201 \pm 7)\ \mu\text{b}$$

we compute the total π^+ photoproduction cross section on ^{6}Li which is presented in Fig. 10.

IV. CRITICISM OF OUR PREVIOUS EXPERIMENT

At this point it is opportune to comment on the deficiencies of our first experiment which lead to an incorrect determination of the ratio a_{Li}/a_p.

A less stringent collimation of the photon beam in our first setup resulted in a larger quantity of stray particles reaching the detectors during the beam burst, producing a comparatively larger

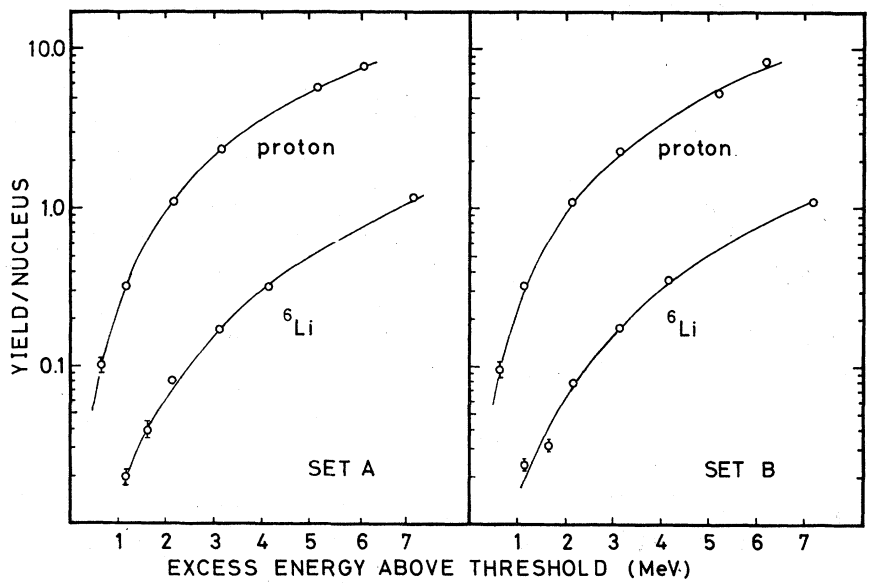

FIG. 9. Measured photoproduction yield per nucleus as a function of the excess energy above threshold for ^{6}Li and hydrogen. The curves indicate the best fit of Eq. (2) to our data.

TABLE II. The theoretical predictions and our results.

Operator	Pion-wave distortion	Nuclear wave function: Configuration of ^{6}He(g.s.)	Nuclear wave function: Radial behavior	$\left(\frac{a(^6\mathrm{Li}\rightarrow{}^6\mathrm{He})}{a(p\rightarrow n)}\right)_{\mathrm{thresh}}$	Ref.
$\vec{\sigma}\cdot\vec{\epsilon}$	Mean optical potential (Krell-Ericson Ref. 21)	SASK A [a]	Phenomenological	0.091	12
		SASK B [b]		0.101	
$\vec{\sigma}\cdot\vec{\epsilon}$	Mean optical potential (Krell-Ericson Ref. 21)	STAN [b]	Harm. Oscil.	0.119	20
		STAN	Saxon-Wood	0.108	
		SASK A	Phenomenological	0.098	
		SASK B		0.109	
		Elementary particle treatment		0.106	
$\vec{\sigma}\cdot\vec{\epsilon}$	Optical potential adjusted to mesic x rays of light nuclei (Ref. 22)	SASK A	Phenomenological	0.097	18
		SASK B		0.108	
Momentum dependent terms included	Optical potential adjusted to mesic x rays of light nuclei (Ref. 22)	SASK A	Phenomenological	0.105	18
		SASK B		0.117	
This experiment ($0<\omega<2$ MeV)				$a(^6\mathrm{Li}\rightarrow{}^6\mathrm{He})/a(p\rightarrow n)=0.098\pm0.004$ [c]	

[a] Strong $L=1$ admixture.

[b] Weak $L=1$ admixture.

[c] Comparing this result with the theoretical predictions, one should recall that it was deduced assuming $a(^6\mathrm{Li}\rightarrow{}^6\mathrm{He})/a(p\rightarrow n)=cte$ in the energy region of interest ($0<\omega<2$ MeV). As discussed in Sec. III C, this approximation has a negligible influence for reasonable variations of $a(^6\mathrm{Li}\rightarrow{}^6\mathrm{He})$ and $a(p\rightarrow n)$.

loading of the photomulipliers for a given beam intensity. Moreover our initial detecting system consisted only of two Lucite Čerenkov counters and high discriminator thresholds had to be used in order to keep the accidental coincidence rate to a reasonable level. Even though the stability of the counting rates against variations of the beam intensity was checked for each target, pulse-height analysis in a subsequent control experiment showed that the CH_2 positron spectrum in the first Čerenkov counter was shifted compared with the Li one. Consequently the interchange of the targets produced an effect on the detectors which was inadequately simulated by the variations of beam intensity we used as a test. Due to the critical influence of the high discriminator threshold a systematic underestimation of the Li yield was introduced relative to the CH_2 one.

Better shielding of our detectors by the introduction of supplementary collimators and an aluminum protective layer (Fig. 2) proved successful to reduce the burden on the photomultipliers which also worked in better conditions due to the utilization of the booster supplies. The use of a third counter allowed us moreover to decrease the detection threshold and so to minimize the influence of any possible gain shift.

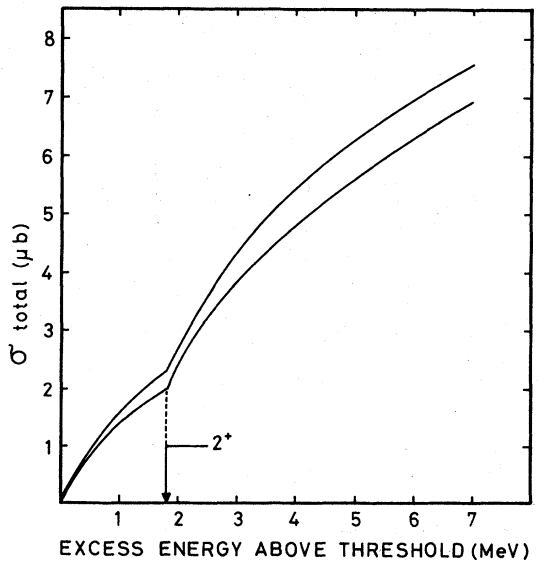

FIG. 10. Cross section of the (γ,π^+) reaction on ^{6}Li deduced from this experiment.

V. CONCLUSION

In Table II we list the most recent estimates of $a(^6\mathrm{Li}\rightarrow{}^6\mathrm{He})/a(p\rightarrow n)$ as well as their main theoretical ingredients. They range from 0.091 to 0.117. As our result, 0.098 ± 0.004 is well within this range, one may conclude that threshold pion photo-

production is well understood within the 4% accuracy of our experiment. One may be tempted, moreover, to discriminate between the models which enter the various predictions. For instance, the Cammarata-Donnelly and Delorme-Figureau predictions, using the "SASK A" configuration and the $\vec{\sigma}\cdot\vec{\epsilon}$ operator alone, perfectly fit our result.

This numerical coincidence is, however, misleading and it seems premature to claim a perfect understanding of the investigated process for the following reasons:

(1) The $\vec{\sigma}\cdot\vec{\epsilon}$ interaction operator is certainly insufficient, even at threshold, because of the Fermi motion of the nucleons. A more complete realistic one, used by Delorme and Figureau,[18] increases, however, the predicted value by 10% and destroys the apparent agreement with experiment.

(2) The many-body effects (other than those taken into account by the distortion of the pion wave) have not been evaluated in the particular case of $A=6$. They are expected to become very important in heavy nuclei.[4]

Some uncertainty continues to prevail also in the nuclear-structure ingredients of the predictions:

(3) In the absence of information on the radial wave function of $^6\mathrm{He}_{g.s.}$, that of the analogous $^6\mathrm{Li}(3.56\ \mathrm{MeV})$ is used. A precise measurement of the $^6\mathrm{Li}_{g.s.} \rightarrow {}^6\mathrm{He}_{g.s.}$ partial muon capture rate should help to control this controversial assumption.[13,20]

(4) It would be essential to distinguish between the SASK A and SASK B descriptions of the ^{6}He configuration. This may be obtained performing precise inelastic electron scattering on ^{6}Li for momentum transfer higher than those investigated up till now.[20]

As a conclusion, further theoretical and experimental work is needed before we may use our result, at its full level of accuracy, to check our understanding of nuclear pion photoproduction at threshold.

The high skill of the Accélérateur Linéaire de Saclay operation group under F. Netter was instrumental to the success of this experiment which required very unconventional beam conditions. The technical contribution of J. Bechade, M. Berger, and G. Ardiot, the help of I. Blomqvist during the data-taking phase of the experiment, and fruitful discussions with J.-L. Faure are gratefully acknowledged. The Louvain group wishes to acknowledge also the friendly hospitality enjoyed at Saclay.

---

†Work partially supported by the Institut Interuniversitaire des Sciences Nucléaires, Belgium.

[1]P. De Baenst, Nucl. Phys. B24, 633 (1970).
[2]M. Ericson and M. Rho, Phys. Rev. C 5, 57 (1972).
[3]M. Moreno, J. Pestieau, and J. Urias, Phys. Rev. C 12, 514 (1975).
[4]J. Delorme, M. Ericson, and G. Fäldt, Nucl. Phys. A240, 493 (1975).
[5]H. W. Baer, K. M. Crowe, and P. Truöl, Advan. Nucl. Phys. (to be published).
[6]P. Truöl, in *Proceedings of the Topical Conference on Meson-Nuclear Physics, Pittsburgh, 1976,* edited by P. D. Barnes, R. A. Eisenstein, L. S. Kisslinger (AIP, New York, 1976), No. 33.
[7]P. Truöl (private communication).
[8]J. H. Koch and T. W. Donnelly, Nucl. Phys. B64, 478 (1973).
[9]C. Tzara, Nucl. Phys. B18, 246 (1970).
[10]J. Deutsch, D. Favart, R. Prieels, B. Van Oystaeyen, G. Audit, N. de Botton, J.-L. Faure, Cl. Schuhl, G. Tamas, and C. Tzara, Phys. Rev. Lett. 33, 316 (1974).
[11]F. Cannata, C. W. Lucas, Jr., and C. W. Werntz, Phys. Rev. Lett. 33, 1316 (1974).
[12]J. C. Bergstrom, I. P. Auer, and R. S. Hicks, Nucl. Phys. A251, 401 (1975).
[13]F. Cannata and C. Werntz, Phys. Rev. C 9, 782 (1974).
[14]P. E. Argan, G. Audit, N. de Botton, J.-L. Faure, J.-M. Laget, J. Martin, Cl. Schuhl, and G. Tamas, Nucl. Phys. A237, 447 (1975).
[15]J. L. Block and J. Mahieux, Nucl. Instrum. Methods 58, 93 (1968).
[16]R. J. Jabbur and R. H. Pratt, Phys. Rev. 129, 184 (1963), footnote 18.
[17]R. J. Jabbur and R. H. Pratt, Phys. Rev. 133, B1091 (1964).
[18]J. Delorme and A. Figureau (private communication).
[19]H. Pilkuhn, W. Schmidt, A. D. Martin, C. Michael, F. Steiner, B. R. Martin, M. M. Nagels, and J. J. de Swart, Nucl. Phys. B65, 460 (1973).
[20]J. B. Cammarata and T. W. Donnelly, Nucl. Phys. A267, 365 (1976).
[21]M. Krell and T. E. O. Ericson, Nucl. Phys. B11, 497 (1969).
[22]L. Tauscher and W. Schneider, Z. Phys. 271, 409 (1974).